

## Threshold production of heavy top quarks: QCD and the Higgs boson

Matthew J. Strassler and Michael E. Peskin

*Stanford Linear Accelerator Center, Stanford University, Stanford, California 94309*

(Received 24 September 1990)

We calculate the threshold cross section for  $e^+e^- \rightarrow t\bar{t}$  to leading-logarithmic order in QCD, using a nonrelativistic approximation suggested by Fadin and Khoze. We study the mass range  $100 \leq m_t \leq 250$  GeV, and show that the cross section is an excellent measure of  $\alpha_s$  for the lower portion of the mass range, while for a heavier top quark it is sensitive to the mass and couplings of the Higgs boson. We argue that a precise determination of  $m_t$  and a measurement of  $\Gamma_t$  are possible. We also show that nonperturbative effects are small, confirming that the  $t\bar{t}$  threshold is a detailed perturbative test of the standard model.

### I. INTRODUCTION

Recent results from Fermilab indicate that if the top quark decays as predicted by the minimal standard model, then it is heavier than 89 GeV.<sup>1</sup> While we await its detection, it is useful to begin thinking about its detailed properties if in fact it is very heavy. For the known heavy quarks  $c$  and  $b$ , it has been exceptionally interesting to study  $e^+e^-$  annihilation near the quark-antiquark threshold, where the nonrelativistic dynamics of quarks in their binding potential produces a rich spectrum of bound states and resonances. The  $t\bar{t}$  threshold region most probably lies beyond the reach of the CERN  $e^+e^-$  collider LEP II, and thus its exploration will be part of the program of a future  $e^+e^-$  linear collider. In addition, the  $t$  mass probably lies near or across a boundary at which a dramatic qualitative change occurs in the nature of the threshold region and the physics issues which it illuminates. In this paper we will analyze the behavior of the  $t\bar{t}$  threshold for top-quark masses in this new regime.

The most striking feature of the  $c\bar{c}$  and  $b\bar{b}$  thresholds is the presence of narrow resonances corresponding to the nonrelativistic bound states of the quark-antiquark pair. The widths of these resonances are controlled by the annihilation of the quark and antiquark to gluons. However, as the mass of a quark increases beyond the mass of the  $W$ , the weak decay of a single quark comes to dominate the width of the bound state, and the familiar structure of the quark-antiquark threshold is destroyed.<sup>2</sup> If the top quark is heavier than the  $W$ , it may decay directly to  $W^+b$ , and its decay width is large and steeply increasing with its mass. Asymptotically, for very large  $m_t$ ,

$$\Gamma_t \sim \frac{G_F}{\sqrt{2}} \frac{m_t^3}{8\pi} = (180 \text{ MeV}) \left( \frac{m_t}{m_W} \right)^3. \quad (1.1)$$

As  $m_t$  is raised from 100 to 200 GeV, the bound-state resonances lose their separate identity and smear together into a broad threshold enhancement.

At first sight, this effect would seem to remove all of the interesting details of the threshold region. However, in a remarkable set of papers, Fadin and Khoze<sup>3</sup> have argued that the large width of a heavy top quark brings in a

new set of fundamental questions. They have pointed out that the top-quark width acts as an infrared cutoff which justifies the use of perturbative QCD. As a result, the variation of the threshold cross section with energy becomes a quantitative prediction of QCD, largely independent of nonperturbative phenomenological considerations, such as the choice of the quark-antiquark potential. Thus the  $t\bar{t}$  threshold region may be identified as the long-sought "hydrogen atom of the strong interactions."<sup>4</sup>

In this paper, following the ideas of Fadin and Khoze, we study in detail the shape of the  $t\bar{t}$  threshold, which is strongly dependent on the value of the  $t$ -quark mass and which exhibits a complex, intricate structure. In carrying out our analysis, we make two improvements in the physics of their calculation which have an important qualitative effect. Since the quark-antiquark potential is close to a Coulomb potential at the short distances relevant for  $t\bar{t}$  binding, Fadin and Khoze in their analysis used the exact solution of the nonrelativistic Coulomb problem. This made it awkward for them to take proper account of the running of the QCD coupling. We will introduce a simple numerical technique which can straightforwardly treat an arbitrary quark-antiquark potential and is thus well suited to including effects of asymptotic freedom. This technique also allows us to include the effect of Higgs-boson exchange on the quark-antiquark potential. Inazawa and Morii<sup>5</sup> have studied the influence of the Higgs-boson-exchange potential for particle-antiparticle systems of heavy leptons and of long-lived heavy quarks, computing the effect of this potential on the spacing of the narrow resonances. We will show that the Higgs-boson-exchange potential is also important for heavy top quarks ( $m_t > 150$  GeV), providing an essential correction to the pure QCD problem and becoming the dominant effect on the  $t\bar{t}$  cross section for  $m_t > 200$  GeV. For  $m_t \leq 150$  GeV, on the other hand, we confirm the result of Fadin and Khoze that the shape of this threshold provides a new and sensitive method of measuring  $\alpha_s$ .

We should warn the reader that our calculation of the  $t\bar{t}$  threshold shape is accurate only to leading-logarithmic order in QCD. As we explain below, we include in our analysis certain specific corrections of order  $\alpha_s$ , but we do not try here to systematically collect all one-loop

QCD corrections. This approximation is adequate for our main purpose, which is to assess the sensitivity of the  $t\bar{t}$  threshold shape to the parameters of the standard model. To extract precise values of  $\alpha_s$  and the properties of the top quark, one should compute the full set of order- $\alpha_s$  corrections. We believe that this is straightforward, and we hope to report the result in a future publication.

We should also remark that, except where we indicate explicitly, our results apply only to the minimal standard model, which contains one physical Higgs boson and no exotic physics. The  $t\bar{t}$  threshold is sensitive to nonstandard Higgs structures and to exotic decay modes of the top quark, through their effects on the top-quark–Higgs-boson Yukawa coupling and the top-quark decay width. We will display this sensitivity through some specific examples in Sec. VII.

This paper is organized as follows: In Sec. II we justify our physical picture by giving a general discussion of the Coulomb problem in QCD and estimating the dependence of the  $t\bar{t}$  production cross section on  $\alpha_s$  and the width of the top quark. Next, we derive the formalism needed for our calculation: In Sec. III we discuss the appropriate nonrelativistic reduction of the Bethe-Salpeter equation to a simple Schrödinger problem, and in Sec. IV we describe our technique for solving this problem numerically. The following sections present the detailed physical assumptions underlying our calculation: In Sec. V we give a careful discussion of the static potential predicted by QCD, and in Sec. VI we discuss the influence of the Higgs boson and explain our treatment of other electroweak effects at the  $t\bar{t}$  threshold. Section VII presents our numerical results, and Sec. VIII contains our conclusions.

While preparing this paper, we received a paper by Kwong<sup>6</sup> which also discusses the top-quark threshold. He has used a method related to ours, and our two papers give similar results. Our approaches are complementary; Kwong is most interested in spectroscopy of the  $1S$  and  $2S$  level spacings, which can only be studied if the top quark is lighter than 120 GeV, while we focus on the shape of the cross section for heavier top quarks, and its sensitivity to  $\alpha_s$  and the Higgs boson. We also received a paper by Feigenbaum<sup>7</sup> which studies the effect of the Higgs boson on toponium production as a function of the Higgs-boson mass, using both an analytic approximation based on the work of Fadin and Khoze and a numerical calculation similar to though less complete than that of Kwong. The results differ quantitatively from ours, though the general conclusions of the two papers are in agreement.

## II. COULOMB PROBLEM AND EFFECTS OF THE TOP-QUARK WIDTH

In order to understand the basic physics of the  $t\bar{t}$  threshold and the relative importance of the various effects which determine its shape, it is useful to quickly review the properties of Coulomb bound states. Consider, then, a particle-antiparticle system bound by a Coulomb potential. This system is characterized by the reduced mass  $\mu = m/2$  and the coupling strength  $\alpha$ .

In the ground state of a nonrelativistic Coulomb system,

$$\frac{p^2}{2\mu} \sim |V(a_0)| \sim \mu\alpha^2, \quad (2.1)$$

for the characteristic radius  $a_0 = (\mu\alpha)^{-1}$ . The relative velocity of the particle and antiparticle is  $\alpha$ , and so relativistic corrections will be of order  $\alpha$ . This implies that we are self-consistent in specializing to the nonrelativistic limit, since our calculation is only intended to be accurate to leading order in  $\alpha_s$ .

Now let us use this estimate quantitatively for a QCD bound state. For the  $t\bar{t}$  system,  $\alpha = \frac{4}{3}\alpha_s$ , where  $\frac{4}{3}$  is the usual SU(3) group theory factor associated with the fundamental representation. The  $S$ -wave states have binding energies

$$E_n = -\frac{\mathcal{R}}{n^2}, \quad (2.2)$$

where the Rydberg  $\mathcal{R} = \frac{4}{9}\alpha_s^2 m_t$ . The radius of the  $n$ th state is  $r_n \sim n^2 a_0$ ,  $a_0 = (\frac{2}{3}\alpha_s m_t)^{-1}$ , and the characteristic velocity is  $v_n \sim \frac{4}{3}\alpha_s/n$ . The ratio of twice the diameter to the velocity is roughly the period of oscillation for  $S$  states:  $(4r_n/v_n) \sim n^3/(\frac{2}{9}\alpha_s^2 m_t)$ . This is a reasonable estimate of the time needed after the  $t$  and  $\bar{t}$  are created for the formation of the bound state. For the ground state, this formation time [evaluated using  $\alpha_s(a_0)$ ] is of order

$$t_{\text{form}} \sim (1 \text{ GeV}^{-1}) \left[ \frac{100 \text{ GeV}}{m_t} \right]. \quad (2.3)$$

In the minimal standard model, the heavy top quark decays almost exclusively to  $W^+b$ , with other decay modes suppressed by Cabibbo-Kobayashi-Maskawa mixing angles. As the mass of the  $t$  increases, the decay rate becomes proportional to the square of the  $t$ -quark–Higgs-boson Yukawa coupling and so increases steeply with  $m_t$ . The width of the  $t$  is 93 MeV at  $m_t = 100$  GeV and goes asymptotically to Eq. (1.1) for large  $m_t$ . (The complete formula<sup>2</sup> appears at the end of Sec. VI.) Models with a nonminimal Higgs sector or other exotic physics may have a substantially different top-quark width; we will discuss this point in Sec. VII.

The lifetimes of previously studied quarkonia were set by annihilation of the quark and antiquark into gluons or photons, since the time scales associated with annihilation were considerably smaller than the lifetimes of the quarks themselves. By contrast, the heavy top quark decays so rapidly that the toponium system decays predominantly to  $W^+W^-b\bar{b}$  via two independent single-quark decays. Decay channels which involve quark-antiquark annihilation (e.g.,  $t\bar{t} \rightarrow W^+W^-, b\bar{b}, H\gamma$ , two gluons, etc.) are suppressed at least by the factor  $|\psi(0)|^2/m_t^3 \sim (a_0 m_t)^3 \sim \alpha_s^3$ , where  $\psi(r)$  is the bound-state wave function. Therefore, as there are no other important decay modes, the width of the toponium resonances will be approximately twice that of the top quark. Furthermore, the lifetime of toponium is so short that the bound states barely have time to form at all.<sup>2,3</sup> In Fig. 1 we compare the lifetime of toponium with the formation

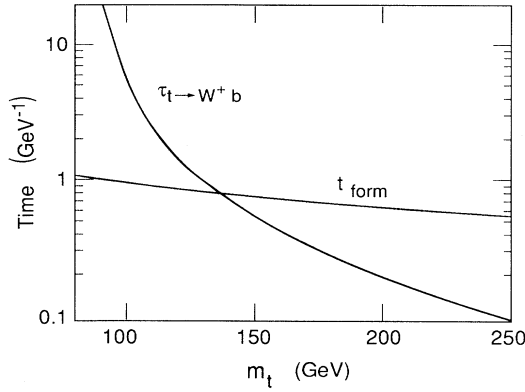


FIG. 1. Comparison of the lifetime ( $2\Gamma_t^{-1}$ ) and the formation time [estimated above, Eq. (2.3)] of the  $1S$  toponium state.

time for the ground state; these cross at  $m_t$  of about 140 GeV. Thus we should expect the distinct toponium states to smear out into a broad threshold structure as  $m_t$  increases, with the  $1S$  resonance, the last to go, disappearing somewhere near  $m_t = 140$  GeV.

There is another interesting effect due to the large width. For  $m_t \sim 120$  GeV or greater, the fact that  $\Gamma_t > \Lambda_{\text{QCD}}$  implies that, in the continuum region above threshold, the  $t$  and  $\bar{t}$  will generally decay *before* hadronization occurs. This permits the decays to be treated perturbatively, allowing a more accurate analysis than is possible for longer-lived quarks.

It is interesting to estimate the dependence of the  $t\bar{t}$  production cross section on  $\alpha_s$  and  $\Gamma_t$ . If the top quark is relatively long lived, so that the cross section can still be described as a sum of sharp resonances, the peak cross section at a resonance is given (in units of  $R$ )<sup>8</sup> by

$$\sigma_{\text{peak}} \sim \frac{1}{m_t^2} \frac{|\psi(0)|^2}{\Gamma_t} R, \quad (2.4)$$

where  $\psi(r)$  is the wave function of the  $t\bar{t}$  bound state. Noting that the wave function at the origin is largest for the ground state ( $n=1$ ) and estimating  $|\psi_1(0)|^2 \approx (a_0)^{-3} \approx (m_t \alpha_s)^3$  in the limit  $\Gamma_t \ll |\mathcal{R}|$ , we find

$$\begin{aligned} \sigma_{\text{peak}} &\sim \frac{1}{m_t^2} \frac{(m_t \alpha_s)^3}{\Gamma_t} R \\ &= \alpha_s^3 \left[ \frac{m_t}{\Gamma_t} \right] R. \end{aligned} \quad (2.5)$$

This indicates a strong sensitivity to  $\alpha_s$  and a swift decrease of the peak height with increasing  $m_t$ , due to the rapid growth of  $\Gamma_t$ . The exact Coulomb calculation<sup>3</sup> shows that for a large width ( $\Gamma_t \gg |\mathcal{R}|$ ), the peak disappears into the continuum, and

$$\sigma \sim \alpha_s^2 \left[ \frac{m_t}{\Gamma_t} \right]^{1/2} R, \quad (2.6)$$

in the region just below threshold. Thus, for larger  $m_t$ , the cross section drops as  $m_t^{-1}$ , as can be seen using (1.1), while the sensitivity of the cross section to  $\alpha_s$  and  $\Gamma_t$  is

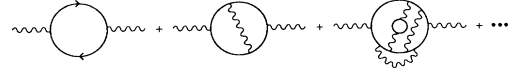


FIG. 2. Diagrams which contribute to  $\Pi_t$ .

less than for lighter top quarks. We will see that leading-logarithmic corrections to the Coulomb approximation do not substantially change this picture.

### III. FORMALISM FOR THE NONRELATIVISTIC APPROXIMATION

We will now present the formalism we need to make this intuitive picture concrete. Because a heavy top quark has no narrow resonances, we should concentrate our attention not on spectroscopy, but on the behavior of the total cross section for top-quark pair production as a function of energy. To leading order in QED, this cross section is given, via the optical theorem, by

$$\sigma(e^+e^- \rightarrow t\bar{t}) = \frac{4\pi\alpha_{\text{QED}}}{s} [-\text{Im}\Pi_t(q^2)], \quad (3.1)$$

where  $\Pi_t(q^2)$  is the top-quark contribution to the photon vacuum polarization. It is straightforward to improve the formula to include the  $Z^0$  and higher-order electroweak corrections, and we will do this in Sec. VI. The more difficult problem is to compute  $\text{Im}\Pi_t(q^2)$ . In this section we reduce this problem to the solution of a nonrelativistic Schrödinger equation. This is a straightforward exercise, which we include to make our assumptions clear.

In perturbation theory,  $\Pi_t(q^2)$  is given by the sum of diagrams shown in Fig. 2. For most values of  $q^2$ , this set of diagrams can be evaluated by directly summing the perturbation expansion. Diagrams containing loops

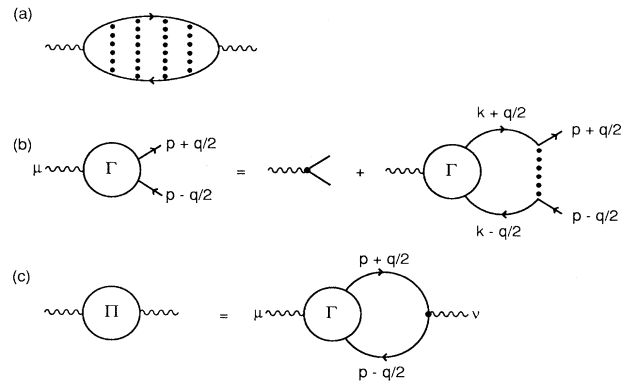


FIG. 3. (a) Diagrams responsible for the leading contribution to  $\Pi_t$  in the nonrelativistic limit; these are the ladder diagrams, involving the exchange of any number of uncrossed gluons. (b) The equation which is satisfied by the vertex function  $\Gamma^\mu$ , in the ladder approximation. (c) The equation which gives  $\Pi_t$  in terms of  $\Gamma^\mu$ .

whose momenta are off shell by an amount  $m_t^2$  are suppressed by factors of  $\alpha_s(m_t^2)$ . However, it is well known that, near threshold, the Coulomb exchange of  $n+1$  bosons between the quark and antiquark is not suppressed relative to the exchange of  $n$  bosons, since the energy denominator from each loop integral contributes a

factor  $\alpha_s^{-1}$ . Thus the leading-order expression for  $\Pi_t(q^2)$  near threshold is the sum of the ladder diagrams shown in Fig. 3(a). These diagrams may be summed by constructing the vector vertex function  $\Gamma^\mu(p, q)$ , which solves the equation shown in Fig. 3(b), and then contracting this vertex function as shown in Fig. 3(c). This gives

$$i(g^{\mu\nu}q^2 - q^\mu q^\nu)\Pi_t(q^2) = \left[ i\frac{2}{3}e \right]^2 \int \frac{d^4p}{(2\pi)^4} \text{tr}[S_F(p+q/2)\Gamma^\mu(p, q)S_F(p-q/2)\gamma^\nu], \quad (3.2)$$

where  $S_F$  is the fermion propagator, and the trace is taken over Dirac and color indices.

To leading order in  $\alpha_s$ , it suffices to analyze the equation for  $\Gamma^\mu$  in the nonrelativistic approximation. Set  $q = (2m_t + E, \mathbf{O})$ , so that  $E$  represents the binding energy of the  $t\bar{t}$  system, and treat all three-momenta as being of order  $\alpha_s$ . Then the fermion propagators may be approximated by their nonrelativistic particle and antiparticle poles:

$$\begin{aligned} S_F(p+q/2) &\rightarrow \frac{i2m_t(1+\gamma^0)/2}{2m_t(E/2+p^0-|\mathbf{p}|^2/2m_t+i\Gamma_t/2)}, \\ S_F(p-q/2) &\rightarrow \frac{-i2m_t(1-\gamma^0)/2}{2m_t(E/2-p^0-|\mathbf{p}|^2/2m_t+i\Gamma_t/2)}. \end{aligned} \quad (3.3)$$

To be consistent with the nonrelativistic expansion, we must ignore in (3.3) the momentum dependence of the imaginary part of the denominator in the quark propagator. We have therefore taken the top-quark width to be constant, evaluating it on the mass shell, using the tree-level standard-model result. This approximation was suggested by Fadin and Khoze.<sup>3</sup>

In the nonrelativistic limit, we need keep only the instantaneous Coulomb part of the gluon propagator. The Coulomb exchange is given to lowest order by

$$(-ig_s)^2(T^a\gamma^0)(T^a\gamma^0)\frac{+i}{|\mathbf{p}-\mathbf{k}|^2}, \quad (3.4)$$

where  $T^a$  is a color-SU(3) representation matrix. We can isolate all terms in the expansion of this form; acting on a color-singlet  $t\bar{t}$  state, they can be combined as  $i(\gamma^0)(\gamma^0)\tilde{V}(\mathbf{p}-\mathbf{k})$ . To leading order,

$$\tilde{V}(\mathbf{p}-\mathbf{k}) = -\frac{4}{3}\frac{4\pi\alpha_s}{|\mathbf{p}-\mathbf{k}|^2}. \quad (3.5)$$

The leading-logarithmic QCD corrections modify this  $(1/r)$  potential by logarithms; we will discuss this effect in Sec. V.

In the nonrelativistic approximation, the equation for  $\Gamma^\mu(p, q)$  in Fig. 3(b) becomes

$$\begin{aligned} \Gamma^\mu(p, q) &= \gamma^\mu + \int \frac{d^4k}{(2\pi)^4} \left[ \frac{1+\gamma^0}{2}\Gamma^\mu(k, q)\frac{1-\gamma^0}{2} \right] \\ &\times \frac{1}{(E/2+k^0-|\mathbf{k}|^2/2m_t+i\Gamma_t/2)(E/2-k^0-|\mathbf{k}|^2/2m_t+i\Gamma_t/2)} \tilde{V}(\mathbf{p}-\mathbf{k}). \end{aligned} \quad (3.6)$$

Since the right-hand side of this equation is independent of  $p^0$ , we may self-consistently take  $\Gamma(k, q)$  independent of  $k^0$ ; then we can perform the  $dk^0$  integration explicitly. A further simplification takes place in the Dirac structure. Inserting (3.3) into (3.2), we see that this integral depends only on  $(1+\gamma^0)\Gamma^\mu(p, q)(1-\gamma^0)$ . Equation (3.6) implies that this component of  $\Gamma^\mu$  takes the form

$$\frac{1+\gamma^0}{2}\Gamma^\mu(p, q)\frac{1-\gamma^0}{2} = \frac{1+\gamma^0}{2}\gamma^\mu\frac{1-\gamma^0}{2}\tilde{\Gamma}, \quad (3.7)$$

where  $\tilde{\Gamma}$  is a scalar function of  $|\mathbf{p}|$  and  $E$ . In all, the equation for  $\Gamma^\mu$  reduces to the scalar equation

$$\begin{aligned} \tilde{\Gamma}(\mathbf{p}, E) &= 1 + \int \frac{d^3k}{(2\pi)^3} V(\mathbf{p}-\mathbf{k}) \frac{1}{(E+i\Gamma_t-|\mathbf{k}|^2/m_t)} \\ &\times \tilde{\Gamma}(\mathbf{k}, E). \end{aligned} \quad (3.8)$$

Let

$$\tilde{G}(\mathbf{k}, E+i\Gamma_t) = -\frac{1}{E+i\Gamma_t-|\mathbf{k}|^2/m_t}\tilde{\Gamma}(\mathbf{k}, E). \quad (3.9)$$

Then we can return (3.8) to coordinate space and see that it is just the Schrödinger equation

$$[H - (E+i\Gamma_t)]G(\mathbf{r}, E+i\Gamma_t) = \delta^{(3)}(\mathbf{r}), \quad (3.10)$$

with

$$H = -\frac{1}{m_t} \nabla^2 + V(\mathbf{r}), \quad (3.11)$$

correctly reflecting the reduced mass of the  $t\bar{t}$  system. We recognize  $G(\mathbf{r}, E)$  as the standard Schrödinger Green's function  $G(\mathbf{r}, \mathbf{r}'; E)$ , evaluated at  $\mathbf{r}'=0$ . As the width of a state is twice the imaginary part of its eigenvalue, we find that the width of the toponium system is  $2\Gamma_t$ , as argued in Sec. II.

The nonrelativistic representation of  $\Gamma^\mu$  that we have just derived can be inserted into the nonrelativistic reduction of (3.2) to provide an expression for  $\Pi_t(E)$ . As in (3.6), the  $dp^0$  integration may be performed explicitly. Then we find

$$\begin{aligned} \Pi_t(E) &= \frac{2}{3} \frac{e^2}{m_t^2} \int \frac{d^3p}{(2\pi)^3} \frac{1}{E + i\Gamma_t - |\mathbf{p}|^2/m_t} \tilde{\Gamma} \\ &= -\frac{2}{3} \frac{e^2}{m_t^2} G(\mathbf{r}=0, \mathbf{r}'=0, E + i\Gamma_t). \end{aligned} \quad (3.12)$$

Inserting this formula into (3.1), we find, for the one-virtual-photon cross section for  $t\bar{t}$  production,

$$\sigma(e^+e^- \rightarrow t\bar{t}) = \frac{8\pi^2 \alpha_{\text{QED}}^2}{3m_t^4} \text{Im}G(0,0; E + i\Gamma_t). \quad (3.13)$$

For  $\Gamma_t=0$ , this equation is easily seen to be equivalent to the standard formula for  $e^+e^-$  production of nonrelativistic bound states. The derivation we have given, following the suggestion of Fadin and Khoze, clarifies that the effect of the top-quark width is to cause the Schrödinger Green's function to be evaluated off the real axis. We will see in the next section that this causes the Green's function  $G(\mathbf{r}, \mathbf{r}'; E + i\Gamma_t)$  to decay exponentially for all values of  $E$ . Thus, if  $\Gamma_t$  is sufficiently large, the calculation of this Green's function will involve only short distances where QCD perturbation theory is valid.

#### IV. METHOD FOR FINDING $\text{Im}G(0,0; E)$

To calculate the total cross section using the formalism of the previous section, we must construct the Green's function of the Schrödinger equation,  $G(\mathbf{r}, \mathbf{r}'; E)$ , evaluated at  $\mathbf{r}=\mathbf{r}'=0$ . This can be done very simply by the technique we will present in this section.

Our basic problem is to solve the second-order inhomogeneous differential equation

$$\left[ -\frac{1}{m_t} \nabla^2 + V(\mathbf{r}) - (E + i\Gamma_t) \right] G(\mathbf{r}, \mathbf{r}'; E + i\Gamma_t) = \delta^{(3)}(\mathbf{r} - \mathbf{r}'). \quad (4.1)$$

Since we will evaluate  $G(\mathbf{r}, \mathbf{r}')$  at the origin, the only relevant contributions will come from  $S$ -wave states. In this partial wave, (4.1) becomes

$$\left[ -\frac{1}{m_t} \left[ \frac{d^2}{dr^2} + \frac{2}{r} \frac{d}{dr} \right] + V(r) - (E + i\Gamma_t) \right] G(r, r') = \frac{1}{4\pi r^2} \delta(r - r'). \quad (4.2)$$

We can simplify the problem by defining

$$g(r, r') = rr' G(r, r'). \quad (4.3)$$

This leads to the one-dimensional Schrödinger equation

$$\left[ \frac{d^2}{dr^2} + m_t [E + i\Gamma_t - V(r)] \right] g(r, r') = \frac{m_t}{4\pi} \delta(r - r'). \quad (4.4)$$

The solution to this equation will be of the form

$$g(r, r') = A g_>(r_>) g_<(r_<), \quad (4.5)$$

where  $r_> = \max(r, r')$ ,  $r_< = \min(r, r')$ , and  $g_>, g_<$  are solutions of the homogeneous equation regular as  $r \rightarrow \infty$ ,  $r \rightarrow 0$ , respectively. Note that, if  $\Gamma_t > 0$ , the solution  $g_>(r)$  decreases exponentially as  $r \rightarrow \infty$ . The constant  $A$  is chosen to give the correct coefficient of the  $\delta$  function; the matching condition is

$$\begin{aligned} \left. \frac{dg}{dr} \right|_{r=r'+\epsilon} - \left. \frac{dg}{dr} \right|_{r=r'-\epsilon} &= -A \mathcal{W}(g_>, g_<; r') \\ &= -\frac{m_t}{4\pi}, \end{aligned} \quad (4.6)$$

where  $\mathcal{W}(f_1, f_2; r) = (f_1 f_2' - f_1' f_2)|_r$  is the Wronskian of two functions  $f_1$  and  $f_2$ . It is well known that, if  $f_1, f_2$  satisfy the Schrödinger equation,  $\mathcal{W}(f_1, f_2)$  is independent of  $r$ .

To go further, let us define two standard solutions to the one-dimensional Schrödinger equation with specified boundary conditions at  $r=0$ . Since  $G(\mathbf{r}, \mathbf{r}')$  must be finite at  $r=0$ , the regular solution for  $g(r)$  must vanish there. Let us define a regular and an irregular solution  $g_0(r), g_1(r)$  satisfying

$$\begin{aligned} g_0(r) &= r + \dots \quad \text{as } r \rightarrow 0, \\ g_1(r) &= 1 + \dots \quad \text{as } r \rightarrow 0. \end{aligned} \quad (4.7)$$

This definition is not complete, because it allows  $g_1$  to contain an arbitrary admixture of  $g_0$ . If  $V(r)$  were regular at the origin, we could impose  $(d/dr)g_1=0$  at  $r=0$ . However, in the case of a Coulomb potential  $g_1(r) = 1 - \beta r \ln(r/d) + \dots$ , where  $\beta$  and  $d$  are constants, and so  $(d/dr)g_1$  diverges as  $r \rightarrow 0$ ; the arbitrariness in the parameter  $d$  induces an arbitrary admixture of  $g_0$  into  $g_1$ . (A similar ambiguity appears for the case of the asymptotically free QCD potential discussed in Sec. V.) Fortunately, it will suffice to impose on  $g_1$  the constraint

$$\text{Im} \left[ \frac{d}{dr} g_1(r) \right] \rightarrow 0 \quad \text{as } r \rightarrow 0, \quad (4.8)$$

which can be maintained for any  $V(r)$  less singular than  $1/r^2$ .

Any  $g_1$  satisfying (4.8) may be chosen, but once it is fixed, we may write the solutions  $g_<(r)$  and  $g_>(r)$  defined in (4.5) as linear combinations of  $g_0$  and  $g_1$ . Since  $g_<(r)$ , like  $g_0$ , must vanish at the origin, we may identify them:

$$g_<(r) = g_0(r). \quad (4.9)$$

The other solution

$$g_>(r) = g_1(r) + Bg_0(r) \quad (4.10)$$

vanishes as  $r \rightarrow \infty$ , which implies

$$B = \lim_{r \rightarrow \infty} \left[ -\frac{g_1(r)}{g_0(r)} \right]. \quad (4.11)$$

Note that while the real part of  $B$  is dependent on the choice of  $g_1$ , the imaginary part is fixed by (4.8).

With these definitions, it is easy to compute the Wronskian at  $r=0$  and to show that  $\mathcal{W}(g_>, g_<) = -1$  and, from (4.6),  $A = -m_t/4\pi$ . We now use (4.3) and (4.5) to write

$$\begin{aligned} G(0,0) &= -\frac{m_t}{4\pi} \lim_{r,r' \rightarrow 0} \frac{g_<(r)}{r} \frac{g_>(r')}{r'} \\ &= -\frac{m_t}{4\pi} \lim_{r' \rightarrow 0} \left[ \frac{g_1(r')}{r'} + B \right]. \end{aligned} \quad (4.12)$$

Using (4.7) and (4.8), we find

$$\text{Im}G(0,0) = -\frac{m_t}{4\pi} \text{Im}B, \quad (4.13)$$

which shows that the ambiguities in the definition of  $g_1$  and  $B$  mentioned above do not appear in the final result.

We have now reduced the computation of the  $t\bar{t}$  production cross section, in the one-virtual-photon approximation, to

$$\sigma(e^+e^- \rightarrow t\bar{t}) = -\frac{2\pi\alpha_{\text{QED}}^2}{3m_t^3} \text{Im}B, \quad (4.14)$$

where  $\text{Im}B$  can easily be computed numerically using (4.11) and the homogeneous version of (4.4).

As a simple application of this formalism, let us compute the production cross section for a nonrelativistic heavy lepton pair. If the lepton mass is about 150 GeV, the width of the lepton will be similar to that of the top quark, while the potential will be negligible. In this case, it is easy to see that (for  $r < r'$ )

$$G(r, r'; E + i\Gamma) = -\frac{m}{4\pi} \frac{\sin\lambda r}{\lambda r} \frac{e^{i\lambda r'}}{r'}, \quad (4.15)$$

where  $\lambda = [m(E + i\Gamma)]^{1/2}$ . Note that this function falls off exponentially for all values of  $E$ , with decay length at most  $\sqrt{2/m\Gamma}$ . Inserting (4.15) into the cross-section formula [and removing from (3.13) the factor  $3 \times (\frac{2}{3})^2$  from the top-quark color and charge], we find

$$\begin{aligned} \sigma(e^+e^- \rightarrow L^+L^-) &= \frac{\pi^2\alpha_{\text{QED}}^2}{2m_L^3} \text{Re}\lambda \\ &= \frac{\pi^2\alpha_{\text{QED}}^2}{2m_L^3} \left[ \frac{(E^2 + \Gamma^2)^{1/2} + E}{2} \right]^{1/2}, \end{aligned} \quad (4.16)$$

where  $E = \sqrt{s} - 2m_L$  is the energy measured from the  $L^+L^-$  threshold. This agrees with Fadin and Khoze<sup>3</sup> for this case.

## V. QCD POTENTIAL

To arrive at a fully self-consistent perturbative result, one needs to calculate all contributions to the  $t\bar{t}$  cross section to a given order in  $\alpha_s$ . There are a very large number of such contributions: corrections to the top-quark width, box diagrams, vertex corrections, crossed gluons, etc. In this paper we will concentrate on the most important source of  $\alpha_s$  dependence, the static potential due to one-gluon exchange, and reserve the full accounting of order- $\alpha_s$  corrections for later work.

However, there is one additional order- $\alpha_s$  correction that is conventionally included in calculations of quarkonium production, and so we will include it here as well. The exchange of a hard gluon at the photon-quark-antiquark vertex corrects the cross section by a factor

$$(1 - 8\alpha_s/3\pi)^2, \quad (5.1)$$

where  $\alpha_s$  must be evaluated at  $2m_t$ .<sup>9,10</sup> This decreases the cross section by about 15%.

Now we will discuss the nonrelativistic potential, which for the  $t\bar{t}$  system is dictated almost completely by perturbative QCD. To lowest order,

$$V(r) = -\frac{4}{3} \frac{\alpha_s}{r}. \quad (5.2)$$

More generally, the static  $q\bar{q}$  potential  $V(r)$  obeys a renormalization-group equation. This equation is solved by replacing  $\alpha_s$  in (5.2) with a running coupling  $\alpha_s(\mu r)$ , where  $\mu$  is a renormalization scale, such that

$$\mu^2 \frac{\partial}{\partial \mu^2} \alpha_s \equiv \beta(\alpha_s) = -\frac{b_0\alpha_s^2}{4\pi} - \frac{b_1\alpha_s^3}{(4\pi)^2} + \dots \quad (5.3)$$

For QCD with  $n_f$  flavors of light quarks,

$$b_0 = 11 - \frac{2}{3}n_f, \quad b_1 = 102 - \frac{38}{3}n_f. \quad (5.4)$$

The solution to Eq. (5.3) with constant coefficients, using the  $\beta$ -function calculated to two loops, is

$$\alpha_s = \frac{4\pi}{b_0 \ln(\Lambda^2 r^2) + (b_1/b_0) \ln[\ln(\Lambda^2 r^2)]}, \quad (5.5)$$

where  $\Lambda$ , which sets the strength of the potential, must be specified by relating it to other parameters of perturbative QCD. In a moment we will consider how to relate  $\Lambda$  to the commonly used parameter  $\Lambda_{\overline{\text{MS}}}$ , where  $\overline{\text{MS}}$  refers to the modified minimal-subtraction renormalization scheme.

First, however, we should remind the reader that  $\Lambda_{\overline{\text{MS}}}$  is defined from  $\alpha_s^{\overline{\text{MS}}}$  at some scale  $Q$  through an equation with the same form as (5.5). Inverting (5.5), one finds

$$\Lambda_{\overline{\text{MS}}} \approx \left[ \frac{4\pi}{b_0\alpha_Q} \right]^{(b_1/2b_0^2)} Q \exp \left[ -\frac{2\pi}{b_0\alpha_Q} \right], \quad (5.6)$$

where  $\alpha_Q \equiv \alpha_s^{\overline{\text{MS}}}(Q^2)$ . It is clear that  $\Lambda_{\overline{\text{MS}}}$  suffers from an ambiguity involving the number of quark flavors in the coefficients of the  $\beta$  function. Physically, it is reasonable that one should take  $n_f$  equal to the number of quarks much lighter than the scale of the relevant physics, and so

we choose  $n_f=5$ . Since the  $t\bar{t}$  wave functions have characteristic radius  $(\alpha_s m_t)^{-1}$ , which lies well between  $m_b^{-1}$  and  $m_t^{-1}$ , the corrections to this choice are small.

However,  $\Lambda_{\overline{\text{MS}}}$  is much more sensitive to experimental uncertainties than  $\alpha_s$  itself, since it appears only in logarithms in any physical amplitude. For this reason, we find it is clearer to express our potential in terms of  $\alpha_s$  in some renormalization scheme at some scale. We choose  $\alpha_Z \equiv \alpha_s^{\overline{\text{MS}}}(m_Z^2)$  as our reference point. Since  $m_b \ll m_Z < m_t$ , the conversion from  $\alpha_Z$  to our potential involves only scales for which  $n_f=5$  is appropriate.

We now return to the task of relating  $\Lambda$  and  $\Lambda_{\overline{\text{MS}}}$ . The energy of a quark-antiquark pair as a function of  $q^2$  was calculated to two gluon loops by Fischler.<sup>11</sup> In the MS scheme, his result is

$$\begin{aligned} \tilde{V}(q, \alpha_s, \mu) = & -\frac{16\pi\alpha_s}{3q^2} \left[ 1 + \frac{3\alpha_s}{4\pi} \left[ \frac{11}{3} \ln(\mu^2/q^2) + \frac{31}{9} \right] \right. \\ & + \left. \left( \frac{3\alpha_s}{4\pi} \right)^2 \left\{ \frac{121}{9} \ln[\ln(\mu^2/q^2)] \right. \right. \\ & \quad \left. \left. + \frac{988}{27} \ln(\mu^2/q^2) + \dots \right\} \right. \\ & \left. + \dots \right]. \end{aligned} \quad (5.7)$$

Billoire<sup>12</sup> extended this to include fermion loops:

$$\tilde{V}(q) = \tilde{V}_{\text{Fischler}} + \left[ \frac{2}{3} \ln(\mu^2/q^2) + \frac{10}{9} \right] n_f + \dots \quad (5.8)$$

(Billoire was also the first to show that nonperturbative effects remain important in studying the threshold behavior of heavy quark systems until the quarks reach a mass of about 100 GeV.) Following Buchmüller, Grunberg, and Tye,<sup>10,13</sup> we take the Fourier transform of (5.7) and (5.8), using

$$\int \frac{d^3\mathbf{q}}{(2\pi)^3} \frac{\ln(q^2)e^{i\mathbf{q}\cdot\mathbf{r}}}{q^2} = -\frac{1}{4\pi r} [\ln(r^2) + 2\gamma_E], \quad (5.9)$$

where  $\gamma_E$  is Euler's constant. The expansion of the result in terms of  $\ln(\mu r)$  can be matched, term by term, with the expansion of (5.5); this allows us to identify

$$\Lambda = \Lambda_{\overline{\text{MS}}} \exp \left[ \frac{C}{2} \right] \approx 2.43 \Lambda_{\overline{\text{MS}}} (n_f=5), \quad (5.10)$$

where

$$C = \frac{1}{b_0} \left[ \frac{31}{3} - \frac{10n_f}{9} \right] + 2\gamma_E. \quad (5.11)$$

Thus the potential is stronger than one might have suspected:

$$|V(r)| > \frac{4}{3} \frac{\alpha_s^{\overline{\text{MS}}}(1/r^2)}{r}. \quad (5.12)$$

This potential is somewhat problematic. It is perturbative and cannot be trusted at distances larger than about

a few tenths of a fermi, where  $\alpha_s$  becomes large. Equation (5.5) even has a pole at

$$\Lambda r_{\text{crit}} = [\ln(\Lambda^2 r_{\text{crit}}^2)]^{b_1/2b_0} \approx 0.785 (n_f=5), \quad (5.13)$$

which is fortunately outside the range of the  $t\bar{t}$  wave functions. We will deal with these problems in a physically motivated but still somewhat *ad hoc* fashion, and will show in our results that wide deviations from our exact choices do not strongly affect our curves, particularly for the higher masses we consider.

First, we perform a simple regulation, replacing

$$\Lambda r \rightarrow f(\Lambda r) = a \tanh \left[ \frac{\Lambda r}{a} \right], \quad (5.14)$$

where  $a$  is an arbitrary number less than the value of  $\Lambda r_{\text{crit}}$  given in (5.13); this eliminates the pole and ensures the potential is smooth. The corrections induced by this replacement are small until  $\Lambda r$  approaches the pole, particularly as the potential depended only on  $\ln(\Lambda r)$ . If  $a$  is taken too large, the potential develops an unphysical dip in the vicinity of the pole; if it is too small, substantial deviations from the perturbative potential appear in the perturbative region. We choose  $a=0.3$  as an intermediate value which minimizes these problems, though, as we will describe in Sec. VII, the effect of changing  $a$  on the observable cross sections is small.

Because of the insensitivity of these cross sections to long-distance effects, we need not be extremely careful in our choice of potential beyond about a fermi. We employ the commonly used prescription that at large distances the potential becomes linear. Buchmüller and Tye have shown<sup>10</sup> that all of the potentials which successfully give the  $c\bar{c}$  and  $b\bar{b}$  bound-state spectra have the same shape in the relevant region of 0.1–1 fm: They are approximately logarithmic with the slope

$$\frac{dV}{d(\ln r)} \sim 0.7 \text{ GeV}. \quad (5.15)$$

This tells us how to match our perturbative potential onto the nonperturbative region in order that it reproduce the known quarkonium spectra. We therefore choose

$$V(r) = \frac{4}{3r} \frac{4\pi}{b_0 \ln[f(\Lambda r)^2] + (b_1/b_0) \ln\{\ln[f(\Lambda r)^2]\}} + Kr, \quad (5.16)$$

with the coefficient  $K$  of the linear term adjusted so that

$$\frac{dV}{d(\ln r)}(r=r_0 \equiv 1.3 \text{ GeV}^{-1}) = 0.733 \text{ GeV}. \quad (5.17)$$

The value 0.773 GeV is taken from Quigg and Rosner;<sup>14</sup> we choose  $r_0=1.3 \text{ GeV}^{-1}=0.26 \text{ fm}$  as an arbitrary matching radius. Our results are insensitive to these particular choices, as we will show later.

Below is a summary of our method for defining the QCD potential. The first four steps are required by per-

turbative QCD; the last two are an *ad hoc* prescription, to which our results are generally insensitive, in which we match our potential onto successful phenomenological potentials for the  $c\bar{c}$  and  $b\bar{b}$  systems. (1) We choose a value for  $\alpha_Z \equiv \alpha_s^{\text{MS}}(m_Z^2)$ ; (2) using  $n_f = 5$ , we compute  $\Lambda_{\overline{\text{MS}}}$  from the formula (5.6); (3) we compute  $\Lambda$  from Eq. (5.10); (4) we take  $\alpha_s$  as in (5.5); (5) we eliminate its pole using (5.14) with  $a = 0.3$ ; and (6) we add to the resulting potential a linear term as in (5.16), choosing  $K$  so as to satisfy Eq. (5.17).

## VI. EFFECT OF THE HIGGS BOSON AND OTHER CORRECTIONS

In addition to the leading-logarithm QCD calculation, we will consider the interesting effect on the static potential of the Higgs boson. Since the Higgs effect is small, of the same order as certain QCD corrections we have ignored, this part of the calculation is not self-consistent; rather, it is intended to be indicative of the magnitude of the effect and of the precision, following a complete calculation, to which the Higgs-boson mass or coupling could be determined from the  $t\bar{t}$  threshold.

It is well known that the effect of scalar exchange between a fermion and an antifermion is to induce an attractive interaction, which in the nonrelativistic limit takes the form of a Yukawa potential. It has been pointed out by Inazawa and Morii<sup>5</sup> that for extremely heavy quarks ( $m_q \sim 500$  GeV) the Higgs interaction would be stronger than that of QCD, and if the quark were sufficiently stable to have well-defined bound states, we would see an enormous enhancement of the quarkonium resonances. However, even without toponium resonances, the Higgs boson can have a large effect on the top threshold region, and this effect is substantial long before the Higgs interaction dominates that of QCD.

For nonrelativistic quarks both gluon and Higgs-boson exchange are approximately static, and we can simply add to the QCD potential of Sec. V the Higgs-boson-mediated Yukawa potential

$$V_H(r) = \frac{g_{tH}^2}{4\pi} \frac{1}{r} e^{-m_H r} = \frac{m_t^2}{4\pi v^2} \frac{1}{r} e^{-m_H r}, \quad (6.1)$$

where  $m_H$  is the Higgs mass,  $g_{tH}$  is the Yukawa coupling of the Higgs boson to the top quark, and  $v = 246$  GeV is the Higgs-field vacuum expectation value. Note that we have used the minimal standard model to evaluate  $g_{tH}$ . If the Higgs boson has a tiny mass, so that the potential it induces is nearly Coulombic out to radii well beyond the Bohr radius of the top quarks, then to leading order the effect of the Higgs boson is simply to increase the strength of the interquark coupling:

$$\frac{4}{3}\alpha_s \rightarrow \frac{4}{3}\alpha_s + \frac{m_t^2}{4\pi v^2}. \quad (6.2)$$

In Fig. 4 we show a comparison of the QCD and Higgs-boson contributions to the  $t\bar{t}$  potential, using  $\alpha_{\text{eff}} = \frac{4}{3}\alpha_s(a_0)$  as an estimate of the gluon coupling. If the cross section in the threshold region is proportional to  $\alpha_s^n$ , we find a relative enhancement for a massless Higgs boson of

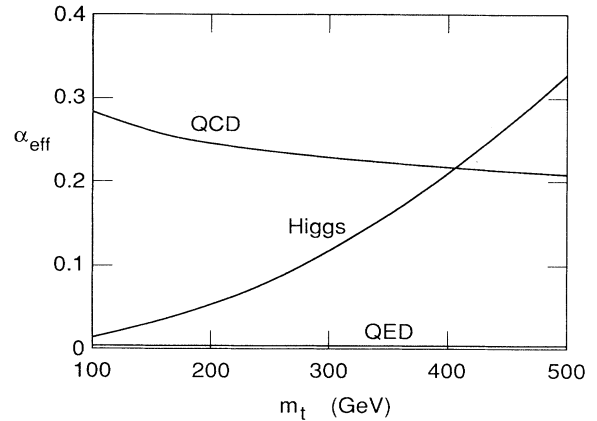


FIG. 4. Comparison, as a function of the top-quark mass, of the effective strength of the QCD, QED, and Higgs-boson interactions between the quark and antiquark at the 1S resonance. The curves are  $\frac{4}{3}\alpha_s(a_0)$  for QCD,  $(\frac{2}{3})^2\alpha_{\text{QED}}$  for QED, and  $(m_t/v)^2/4\pi$  for the Higgs boson. The last curve is appropriate for a massless Higgs boson; the real Higgs-boson effect is somewhat smaller.

$$\frac{\Delta\sigma}{\sigma} \sim \frac{3n}{16\pi} \frac{m_t^2}{\alpha_s v^2} \sim (20\%)n \left[ \frac{m_t}{200 \text{ GeV}} \right]^2. \quad (6.3)$$

The estimate (2.6) shows that  $n$  lies between 2 and 3 for the region of interest. [For very large quark masses in the 500-GeV range, one may use (2.6) to estimate that the cross section, in units of R, grows as  $m_t^2$ ; in real terms it goes to a constant.] On the other hand, as the Higgs boson becomes more massive, the range and influence of its Yukawa potential are reduced. Thus the size of the Higgs-boson correction to the cross section is a measure of the Higgs-boson mass.

One might ask whether  $Z^0$  or photon exchange might also produce a substantial effect. The answer is no: The photon correction is of order  $\alpha_{\text{QED}} < \alpha_s^2$ , and the  $Z^0$  vector coupling to the  $t$  quark is smaller than  $\alpha_{\text{QED}}$  by the factor

$$\frac{(1 - \frac{8}{3}\sin^2\theta_W)^2}{16\cos^2\theta_W\sin^2\theta_W} = 0.048. \quad (6.4)$$

The  $Z^0$  axial-vector coupling is also unimportant, because the axial-vector coupling is momentum and spin dependent and thus is suppressed in the nonrelativistic limit.

Though electroweak corrections to the  $t\bar{t}$  potential are very small, there are four other electroweak effects which are important in the determination of the total cross section for  $e^+e^- \rightarrow t\bar{t}$ .<sup>15</sup> All of these effects were included in the analysis of Fadin and Khoze.<sup>3</sup> The first of these is the effect of  $e^+e^-$  annihilation through a  $Z^0$ , which we have neglected in our formulas from (3.1) onward, but which is easy to reintroduce. The  $Z^0$  current has both vector and axial-vector pieces. However, the axial-vector

coupling to  $t\bar{t}$ , which produces only  $P$ -wave states, can be neglected, since the amplitude for producing such states contains an extra power of the quark three-momentum, suppressing their production by a factor  $\alpha_s^2$ . The vector coupling on the electron side, which is proportional to the small quantity  $(\frac{1}{4} - \sin^2\theta_W)$ , is also negligible. Thus the photon- and  $Z^0$ -exchange contributions do not interfere, and the  $Z^0$  may be included simply by replacing

$$\left[\frac{2}{3}\right]^2 \rightarrow \left[\left[\frac{2}{3}\right]^2 + \left[\frac{(1 - \frac{8}{3}\sin^2\theta_W)}{16\sin^2\theta_W\cos^2\theta_W} \frac{s}{s - m_Z^2}\right]^2\right], \quad (6.5)$$

in (3.1) and subsequent formulas.

The second important effect is the renormalization-group running of  $\alpha_{\text{QED}}$ . Since the  $t\bar{t}$  production cross section is proportional to  $\alpha_{\text{QED}}^2$ , with this coupling constant evaluated at the scale  $s \sim (4m_t^2)$ , we should multiply our formula for the cross section by<sup>16</sup>

$$\left[\frac{\alpha_{\text{QED}}(4m_t^2)}{\alpha_{\text{QED}}(0)}\right]^2 = \left[\frac{137.0}{127.1 - 1.415 \ln(2m_t/300 \text{ GeV})}\right]^2, \quad (6.6)$$

which involves a 15% increase.

The third important electroweak effect is that of initial-state radiation, which can reduce the center-of-mass energy in the  $e^+e^-$  collision and thereby move the virtual  $Z^0$  or  $\gamma$  below  $t\bar{t}$  threshold. It is well known, from theoretical studies of the  $Z^0$  line shape, that initial-state radiation decreases the peak cross section of a resonance by a substantial amount; it is a 25% reduction for the  $Z^0$ , but of order 50% for the low-mass toponium resonances, due in part to their smaller width. In the calculations reported here, we have used the formalism of Kuraev and Fadin,<sup>17</sup> which views the initial-state photons as arising from an electron structure function. Working to first order in  $\alpha_{\text{QED}}$  and to all orders in collinear radiation, we write the measured cross section  $\sigma(s)$  in terms of the uncorrected cross section  $\sigma_0(s)$  as

$$\sigma(s) = \left[1 + \frac{2\alpha_{\text{QED}}}{\pi} \left[\frac{\pi^2}{6} - \frac{1}{4}\right]\right] \int_0^1 dx [\beta x^{\beta-1} (1 + 3\beta/4) - \beta(1-x/2)] \sigma_0[s(1-x)], \quad (6.7)$$

where

$$\beta = \frac{2\alpha_{\text{QED}}}{\pi} \left[\ln \frac{s}{m_e^2} - 1\right] \approx 0.11. \quad (6.8)$$

Here  $m_e$  is the electron mass, and since the radiated photons are at low energy in the electron frame,  $\alpha_{\text{QED}}$  takes its low-momentum value of about  $\frac{1}{137}$ . For a full explication of this formula, the reader should consult reviews of the  $Z^0$  line-shape problem (e.g., Refs. 18 and 19).

Finally, the  $t\bar{t}$  production cross section depends sensitively on the value of the top-quark width. Except where it is noted below, we have used the formula of the minimal standard model:<sup>2</sup>

$$\Gamma_t = \frac{G_F m_t^3}{8\sqrt{2}\pi} |V_{tb}|^2 \left[\frac{2k}{m_t}\right] \left[\left[1 - \frac{m_b^2}{m_t^2}\right]^2 + \left[1 + \frac{m_b^2}{m_t^2}\right] \frac{m_W^2}{m_t^2} - 2\frac{m_W^4}{m_t^4}\right], \quad (6.9)$$

where  $k$  is the three-momentum of the decay products in the  $t$  rest frame. The asymptotic form of this expression has been quoted in (1.1). We approximate  $|V_{tb}| = 1$  in most of what follows.

We have now presented all the details of our prescription for computing the cross section for  $t\bar{t}$  production in high-energy  $e^+e^-$  colliders. Let us summarize this procedure. We will express  $e^+e^-$  cross sections in units of  $R$  throughout the following discussion.<sup>8</sup> In these units the cross section for  $t\bar{t}$  production, without initial-state radiation, is given by (4.14), as modified by (5.1), (6.6), and (6.5):

$$\sigma_0(s) = \frac{2}{m_t} \left[1 - \frac{8}{3} \frac{\alpha_s}{\pi}\right]^2 \left[\frac{\alpha_{\text{QED}}(4m_t^2)}{\alpha_{\text{QED}}(0)}\right]^2 \left[1 + \left[\frac{3(1 - \frac{8}{3}\sin^2\theta_W)}{32\cos^2\theta_W\sin^2\theta_W} \frac{s}{s - m_Z^2}\right]^2\right] (\text{Im}B) R, \quad (6.10)$$

where  $B$  is computed from (4.4) and (4.11) using (5.16), (6.1), and (6.9). The final cross section is then obtained by inserting (6.10) into (6.7) to account for initial-state radiation.

## VII. RESULTS

In this section we present our results on the  $t\bar{t}$  cross section as we vary the parameters of our model. For most of this section, we will work within the minimal ver-

sion of the standard model and consider the effect of varying  $m_t$ ,  $m_H$ , and  $\alpha_s$ . At the end of the section, we will consider the effects of nonminimal Higgs-boson couplings and of modifications of the top-quark width.

The numerical programs used for these calculations were carefully checked. Each of us wrote an independent program, and our final results agree to better than 1%, far less than uncertainties due to QCD corrections. For a pure Coulomb potential without initial-state radiation, our programs agree with the exact analytic result to 1

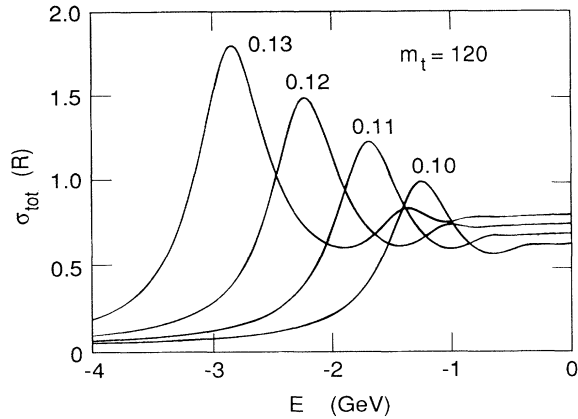


FIG. 5. Total cross section  $\sigma(e^+e^- \rightarrow t\bar{t})$  vs center-of-mass energy, taking  $m_t = 120$  GeV and  $m_H = \infty$ , for  $\alpha_s^{\text{MS}}(m_Z^2) = 0.10, 0.11, 0.12,$  and  $0.13$ . The cross section is measured in units of  $R$ , and the energy is measured from twice the top-quark mass:  $E = \sqrt{s} - 2m_t$ .

part in  $10^5$ .

Before discussing the figures, we should mention that even with little additional knowledge about  $\alpha_s$  or  $m_H$  and with only a few hundred events, a measurement of  $m_t$  to  $\frac{1}{2}$  GeV or better should be possible; this has been confirmed in recent Monte Carlo studies by Komamiya.<sup>20</sup> This measurement can be compared with other determinations of  $m_t$  as a test of QCD radiative corrections.

We begin by surveying the effect of variations in  $\alpha_s \equiv \alpha_s^{\text{MS}}(m_Z^2)$  and  $m_H$ , within the minimal standard model, for various values of  $m_t$ . In Figs. 5–12, we display this dependence for four values spanning the allowed range of  $m_t$ : 120, 150, 180, and 210 GeV. For each of these values, we show the effect of varying  $\alpha_s$  from 0.10 to 0.13, ignoring the effect of the Higgs boson (equivalent to setting  $m_H$  infinite), and also the effect, for  $\alpha_s$  fixed at 0.12, of varying the Higgs-boson mass, using  $m_H = 40, 100, 200$  GeV, and infinity. In all cases, the en-

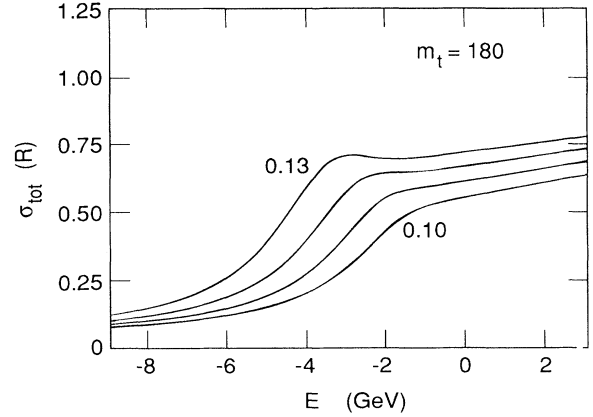


FIG. 7. Total cross section for  $t\bar{t}$  production, with  $m_t = 180$  GeV. The notation is as in Fig. 5.

ergy on the horizontal scale is the center-of-mass energy  $E$  measured from  $2m_t$ , and the vertical scale gives the radiatively corrected cross section, in units of  $R$ .

As we argued in Sec. II, the cross section at the 1S peak is highly sensitive to  $\alpha_s$  for  $m_t < 150$  GeV and becomes less so as the mass increases. This can be seen by inspection of Figs. 5–8. Figure 5 shows that for  $m_t = 120$  GeV, a 10% variation in  $\alpha_s$  makes a 20–25% difference in the peak cross section and a 30–35% change in the binding energy  $E$  at the peak. For 150 GeV (Fig. 6) a 10% increase in  $\alpha_s$  changes  $\sigma_{\text{peak}}$  by only 15–20%, and the energy at the peak by 35–40%. As expected,  $\sigma_{\text{peak}}$  drops rapidly with  $m_t$ , falling from 1.5 to 0.8 units of  $R$  for  $\alpha_s = 0.12$  as  $m_t$  goes from 120 to 150 GeV. By 180 GeV the peak has essentially disappeared, but still the sensitivity of the cross section is large enough to allow a good measurement of  $\alpha_s$ . Some supplementary information comes from the region well above the peak, but here the dependence on  $\alpha_s$  is weaker; a 10% increase in  $\alpha_s$  increases the cross section by 5–10% for all of the masses we consider. However, for the higher values of  $m_t$ , the cross section above threshold has a significant slope, so that  $\alpha_s$  cannot be determined just from this region unless

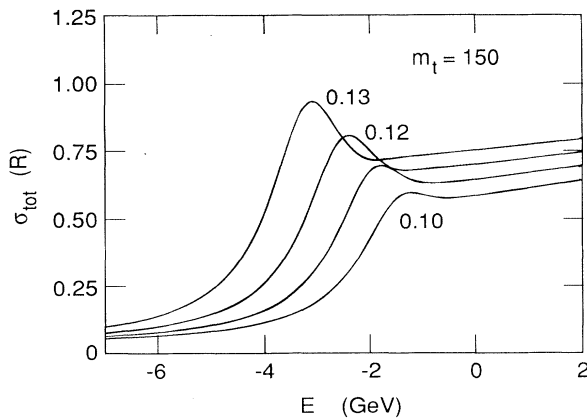


FIG. 6. Total cross section for  $t\bar{t}$  production, with  $m_t = 150$  GeV. The notation is as in Fig. 5.

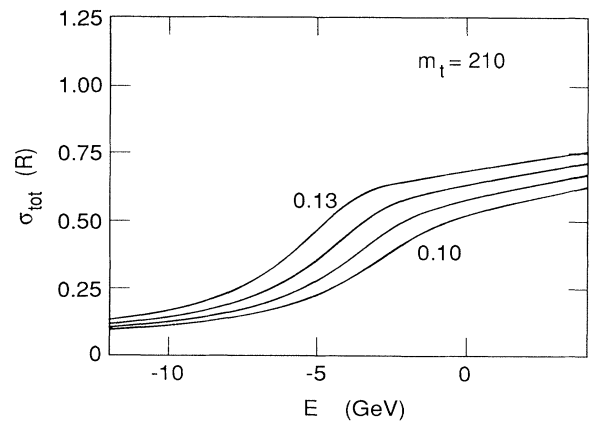


FIG. 8. Total cross section for  $t\bar{t}$  production, with  $m_t = 210$  GeV. The notation is as in Fig. 5.

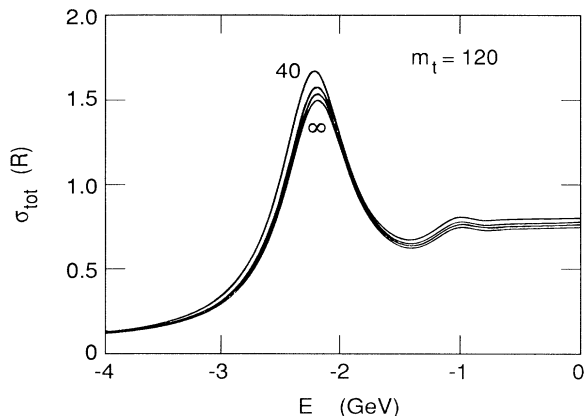


FIG. 9. Total cross section  $\sigma(e^+e^- \rightarrow t\bar{t})$  vs center-of-mass energy, taking  $m_t = 120$  GeV and  $\alpha_s^{\overline{\text{MS}}}(m_Z^2) = 0.12$ , for  $m_H = 40, 100, 200$  GeV, and infinity. The cross section is measured in units of R, and the energy is measured from twice the top-quark mass:  $E = \sqrt{s} - 2m_t$ .

$m_t$  is known to high precision from fitting the region below threshold. The area under the curve may prove to be the most useful quantity for determining  $\alpha_s$  at these higher masses.

The effect of Higgs-boson exchange on the cross section can be seen in Figs. 9–12. The cross section for  $m_t = 120$  GeV depends weakly on  $m_H$ , showing only a 10% variation in  $\sigma_{\text{peak}}$  and unmeasurable variations off the peak for the Higgs-boson masses chosen. Such an effect can be mimicked by a small increase in both  $\alpha_s$  and  $m_t$ , and is therefore undetectable. The situation improves rapidly, however; already by  $m_t = 150$  GeV there is an overall 15% difference in the cross section between the cases of a light and a heavy Higgs boson. This difference grows to about 35% for  $m_t = 210$  GeV. It should be noted that Higgs-boson effects come to dominate uncertainties in  $\alpha_s$  for  $m_t \geq 180$  GeV, as can be seen from the figures.

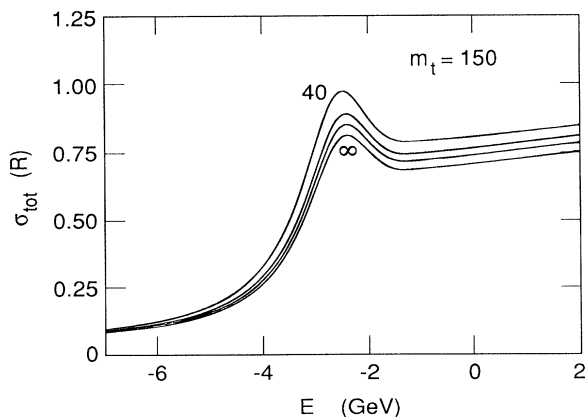


FIG. 10. Total cross section for  $t\bar{t}$  production, with  $m_t = 150$  GeV. The notation is as in Fig. 9.

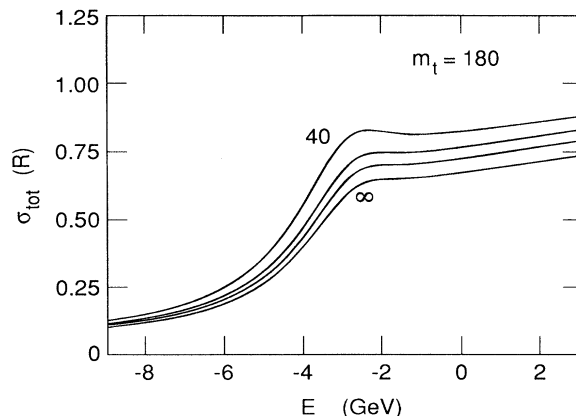


FIG. 11. Total cross section for  $t\bar{t}$  production, with  $m_t = 180$  GeV. The notation is as in Fig. 9.

For the sake of amusement, we have included a graph of the effect of the Higgs boson on a top quark of 450 GeV in Fig. 13. At this mass the Yukawa coupling has grown larger than  $\alpha_s$ . Note that though the cross section is larger in units of R than for  $m_t = 210$  GeV, it is smaller in real terms. Still, the effects of the Higgs-boson mass are enormous.

It is important to check that the results we have presented are not significantly affected by our treatment of the nonperturbative effects in the quark-antiquark potential. In fact, all of our results are quite insensitive to reasonable changes in the parameters  $K$ ,  $r_0$ , and  $a$  defined at the end of Sec. V. Figure 14 shows the effect of making a large change in the slope of the potential in the nonperturbative region (equivalent to changing either  $K$  or  $r_0$ ), for the case of a 100-GeV top quark. In this figure, we have plotted the  $1S$  peak using our standard potential for  $\alpha_Z = 0.11$ , and the cross sections for  $\alpha_Z = 0.12$  using three different values for the slope (5.17) in the nonperturbative region:  $dV/d(\ln r) = 0.333, 0.733, \text{ and } 1.133$  GeV. Since this quantity is known to about 10%,<sup>10</sup> the

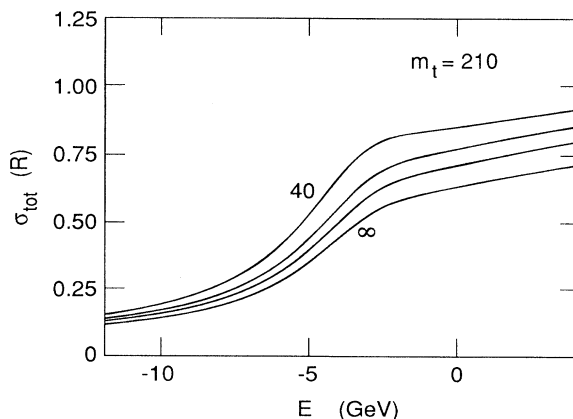


FIG. 12. Total cross section for  $t\bar{t}$  production, with  $m_t = 210$  GeV. The notation is as in Fig. 9.

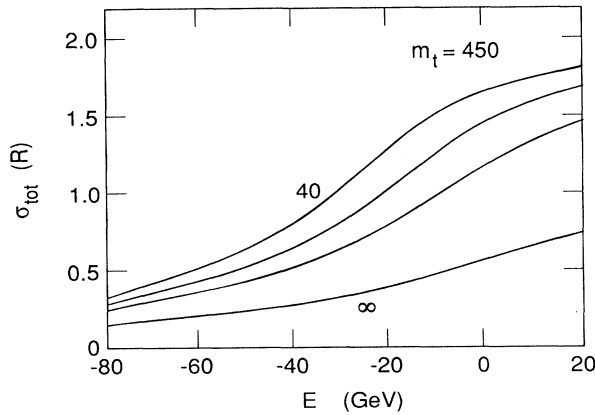


FIG. 13. Total cross section for  $t\bar{t}$  production, with  $m_t = 450$  GeV. The notation is as in Fig. 9.

above range of values far exceeds the experimental uncertainties. The line shape is noticeably sensitive to  $K$  in the region of the  $2S$  and  $3S$  states. This is because the excited states have a larger radius and sample the potential further from the origin than the ground state. The spacings between the states, as well as the peak heights, are very sensitive to the shape of the long-range potential; the analysis of Kwong<sup>6</sup> takes advantage of this fact. However, the shape and position of the  $1S$  peak varies by only 5% under these changes in  $K$  and remains a perturbative prediction. The figure makes clear that, because of their weak dependence on the nonperturbative part of the potential, the height and position of the peak are precise measures of  $\alpha_s$  for  $m_t \geq 100$  GeV.

For larger  $m_t$ , the peaks of the excited states broaden until they are no longer visible. What this means is that the increasing top-quark width (more than its increasing

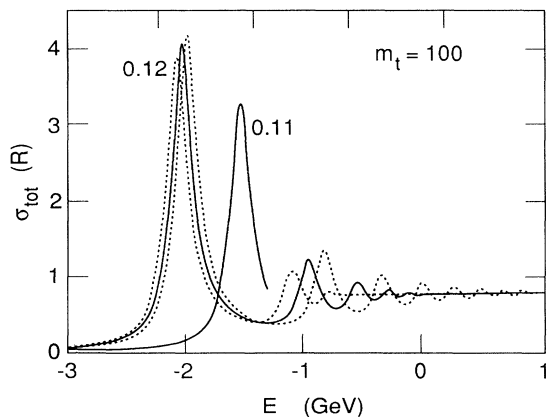


FIG. 14. Total cross section  $\sigma(e^+e^- \rightarrow t\bar{t})$  vs center-of-mass energy, taking  $m_t = 100$  GeV and  $m_H = \text{infinity}$ , showing the effect of varying the slope of the potential at large distances. The isolated peak has  $\alpha_s^{\text{MS}}(m_Z^2) = 0.11$ ; the clustered curves have  $\alpha_s^{\text{MS}}(m_Z^2) = 0.12$  with slope [see Eq. (5.17)]  $dV/d(\ln r_0) = 0.333, 0.733, \text{ and } 1.133$ . The cross section is measured in units of  $R$ , and the energy is measured from twice the top-quark mass:  $E = \sqrt{s} - 2m_t$ .

mass) cuts off the wave functions before they have a chance to sample the nonperturbative region, and the entire threshold cross section becomes perturbative. The unphysically large variations of  $dV/d(\ln r)$  used in Fig. 14 give deviations of only 3% in the peak height and the Rydberg for  $m_t = 120$  GeV and 1% for  $m_t = 150$  GeV.

The cross-section calculations show a similar variation when the regulator parameter  $a$ , defined in (5.14), is varied in the range 0.2–0.5. For values of  $a$  as large as 0.5, the potential is badly distorted at large distances, but as suggested before, our result for the cross section is quite insensitive to this region. For values of  $a$  smaller than 0.3, the infrared cutoff begins to flatten the potential in the perturbative region. This modification of the potential at short distances does affect our numerical results, but its effects, although no larger than perturbative QCD corrections, are not physical and carry us outside the realm of a systematic calculation. To be conservative, we use the variation in our calculated cross sections from  $a = 0.3$  to 0.2 as a measure of the uncertainty in these cross sections due to nonperturbative physics. We thus estimate an uncertainty from this source of 2% at  $m_t = 120$  GeV, 1% at  $m_t = 150$  GeV, and still less for larger values of  $m_t$ . The variation of  $K$  within physically reasonable limits leads to an even smaller systematic uncertainty. Overall, these ambiguities should be much smaller than the uncertainties from perturbative QCD corrections, since even when the order- $\alpha_s$  contributions are known, order- $\alpha_s^2$  corrections of a few percent will remain.

A precision measurement of the shape of the  $t\bar{t}$  threshold cross section thus gives information on three fundamental parameters of the standard model:  $m_t$ ,  $m_H$ , and  $\alpha_s$ . How the data will be used to constrain these parameters will depend on what other experimental data are available at that time. In the next few years, experiments at the  $Z^0$  should yield a measurement of  $\alpha_s^{\text{MS}}(m_Z^2)$  with an accuracy of  $\pm 0.005$ .<sup>21</sup> As for the top quark, if it is sufficiently light, it should be discovered at the Fermilab Tevatron collider and its mass measured to  $\pm 10$  GeV. High-energy experiments at an  $e^+e^-$  linear collider which reconstruct top quarks above threshold can probably improve this accuracy to better than 1 GeV. Meanwhile, the Higgs boson, if standard, will be discovered at LEP II, the Superconducting Super Collider and/or an  $e^+e^-$  linear collider, assuming its mass is low enough to be important to the  $t\bar{t}$  threshold problem. Within this context, then, the measurement of the  $t\bar{t}$  threshold cross section will serve as a method of improving the precision determination of  $\alpha_s$  and  $m_t$  while providing confirmation of the existence and standard behavior of the Higgs boson through its virtual effects. The question of how to extract  $\alpha_s$ ,  $m_t$ , and/or  $m_H$  from these curves is a subtle and difficult one, which is strongly dependent on  $m_t$ . A first analysis is given by Komamiya in Ref. 20.

We may hope, however, that the minimal standard model will not completely describe the physics of the top-quark–Higgs-boson system. In this case, the measurement of the  $t\bar{t}$  threshold can make two important contributions to the experimental unraveling of the top

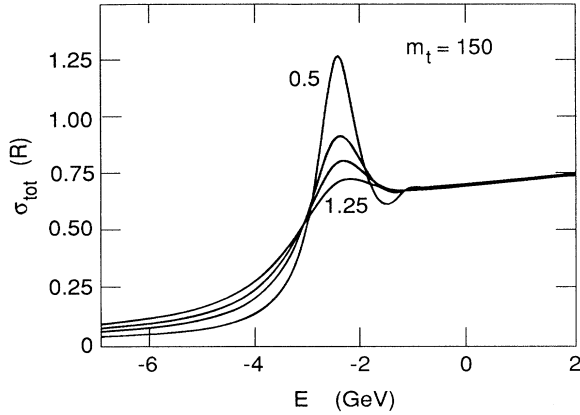


FIG. 15. Effect of the width of the top quark on the  $t\bar{t}$  cross section. Total cross section  $\sigma(e^+e^- \rightarrow t\bar{t})$  vs center-of-mass energy, taking  $m_t = 150$  GeV,  $m_H = \text{infinity}$ , and  $\alpha_s^{\text{MS}}(m_Z^2) = 0.12$ , for  $\Gamma_t = 0.5, 0.8, 1.0$ , and  $1.25$  times its standard-model value [Eq. (6.9), with  $|V_{tb}| = 1$ ]. The cross section is measured in units of R, and the energy is measured from twice the top-quark mass:  $E = \sqrt{s} - 2m_t$ .

quark interactions. First, this experiment allows a direct measurement of the lifetime of the top quark. In modified versions of the standard model, the top-quark width can either decrease or increase relative to its standard value. If there is a fourth generation of heavy quarks,  $|V_{tb}|^2$  may be substantially less than 1; as given in Eq. (6.9), this would reduce  $\Gamma_t$ . On the other hand, if new particles appear with masses below  $m_t$ , this will provide new decay channels which will increase the width of the top quark. If there exists a charged Higgs boson with mass comparable to the  $W$  boson, the ratio of the decay rates for  $t \rightarrow W^+b$  and  $t \rightarrow H^+b$  is of order 1, depending on the mixing angles of the nonminimal Higgs sector. If there exists a supersymmetric partner  $\tilde{t}$  of the top quark, then, if the kinematics allow, supersymmetric decays such as  $t \rightarrow \tilde{t}\tilde{\gamma}$  may be important. In these and other scenarios, the top-quark width can be substantially larger than the value (6.9).

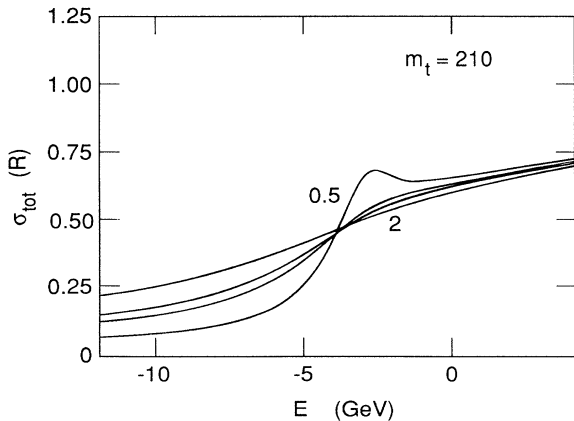


FIG. 16. Effect of the width of the top quark on the  $t\bar{t}$  cross section, with  $m_t = 210$  GeV and  $\Gamma_t = 0.5, 1.0, 1.25$ , and  $2.0$  times its standard-model value. The notation is as in Fig. 15.

To show how this modification would affect the  $t\bar{t}$  threshold cross section, we have presented in Figs. 15 and 16, for  $m_t = 150$  and  $210$  GeV, a comparison of the threshold structure for various values of  $\Gamma_t$ . Both figures show that the important effects occur around and below the visible resonance, as it becomes narrow or broad; the cross section near and above threshold, which is featureless and almost flat, is barely altered by changes in  $\Gamma_t$ . For  $150$  GeV, cutting the width in half adds more than 50% to the height of the peak; a 20% reduction in the width means a 15% enhancement of the peak cross section, while a 25% increase in the width reduces  $\sigma_{\text{peak}}$  by only 10%. For  $m_t = 210$  GeV, a width equal to one-half the standard-model prediction restores the peak; by contrast, doubling the width substantially increases the cross section below the peak. However, at this mass, variations of order 25% in the width make changes in the cross section which will be very difficult to detect; they are only a few percent in the region of the resonance and slightly larger at lower energies where the measurements are more difficult because of the lower collision rate. We can conclude that sensitivity to changes in  $\Gamma_t$  is dependent on the prominence of toponium resonances and is therefore greater for low  $m_t$ . (It is worth noting that  $\Gamma_t$  is the only parameter which increases the cross section in some regions while decreasing it in others, so that the effect of a change in  $\Gamma_t$  cannot be imitated by changing  $m_t$ ,  $m_H$ , and  $\alpha_s$  in combination.)

It is also of great importance to measure the coupling  $g_{tH}$  of the Higgs boson to the top quark. Any deviation of this coupling from its value in the minimal standard model,

$$g_{tH}^{\text{SM}} = \frac{m_t}{246 \text{ GeV}}, \quad (7.1)$$

is a sign of a more complicated Higgs sector. In Fig. 17, using  $m_t = 150$  GeV, we fix  $\alpha_s = 0.12$  and  $m_H = 100$  GeV and show the effect of taking  $g_{tH}/g_{tH}^{\text{SM}} = 0, 0.5, 1.0$ , and

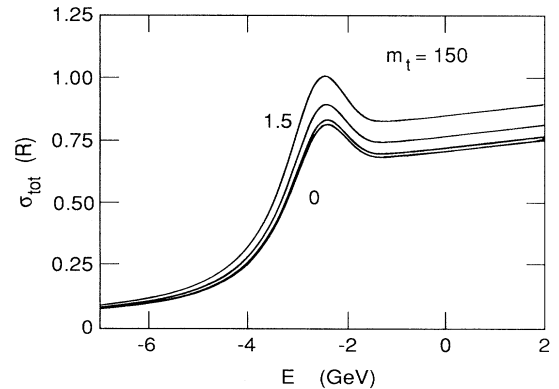


FIG. 17. Effect of the top-quark-Higgs-boson coupling  $g_{tH}$  on the  $t\bar{t}$  cross section. Total cross section  $\sigma(e^+e^- \rightarrow t\bar{t})$  vs center-of-mass energy, taking  $m_t = 150$  GeV,  $m_H = 100$  GeV, and  $\alpha_s^{\text{MS}}(m_Z^2) = 0.12$ , for  $g_{tH}/g_{tH}^{\text{SM}} = 0, 0.5, 1.0$ , and  $1.5$  times its standard-model value [Eq. (7.1)]. The cross section is measured in units of R, and the energy is measured from twice the top-quark mass:  $E = \sqrt{s} - 2m_t$ .

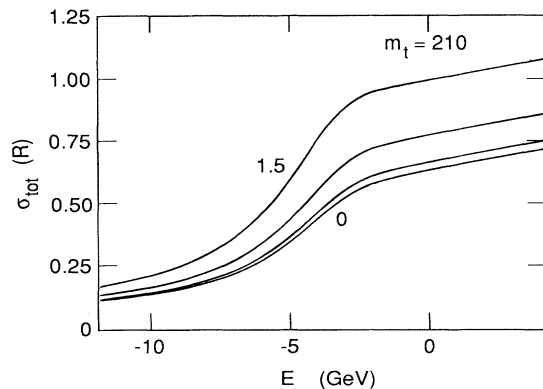


FIG. 18. Effect of the top-quark-Higgs-boson coupling  $g_{tH}$  on the  $t\bar{t}$  cross section, with  $m_t = 210$  GeV. The notation is as in Fig. 17.

1.5. In Fig. 18 we do the same for  $m_t = 210$  GeV. The change in the cross section due to the Higgs boson is approximately quadratic in the top-quark-Higgs-boson coupling, as was argued above [see Eq. (6.3)]. The effect is systematic, so that the area under the curve may be used in the measurement, decreasing the statistical errors substantially. We may therefore hope that the top-quark threshold will provide one of the few available tests of the coupling of the Higgs-boson and fermion sectors of the standard model.

### VIII. SOME CONCLUDING COMMENTS

The measurement of the  $t\bar{t}$  cross section raises a number of experimental problems, which we have not studied in detail. An initial analysis of this system has been done by Komamiya.<sup>20</sup> We limit ourselves to some general comments. The greatest experimental problem for this measurement is obtaining both high luminosity and small beam spread. Since the cross sections are of order one unit of R, the rates will be low,<sup>8</sup> and so careful consideration will have to be given to the method of scanning the threshold region in order to best extract the relevant physical quantities. Fortunately, efficiencies for detecting  $t\bar{t}$  events should be high because of the characteristic kinematics of the decay  $t \rightarrow Wb$ . In addition, other physics studies, such as the measurement of the  $WW\gamma$  vertex and the searches for the Higgs boson and other new particles,

can be done simultaneously with the scan of the  $t\bar{t}$  threshold.

We remind the reader that our results are only accurate to leading-logarithmic order in QCD. They contain several effects which, though higher order, are important corrections: Higgs-boson exchange, initial-state radiation of photons, the running of  $\alpha_{\text{QED}}$ , and the hard-gluon correction to the  $\gamma t\bar{t}$  vertex. We use the full one-loop corrections to the QCD potential, but treat the potential as static (energy independent) and take the top quarks to be nonrelativistic. Clearly, there are many corrections to our results which must be considered, some of which may be substantial; we intend to perform the full order- $\alpha_s$  calculation in the future.

Nevertheless, our results clearly show that the study of the  $t\bar{t}$  threshold will be a fruitful one. Exactly what will be learned from this study depends in detail on what will be known from other experiments, and one can best view it as providing increasingly strong constraints in a multidimensional parameter space. It will certainly be possible to make high-precision correlated measurements of  $m_t$  and  $\alpha_s$  with relatively few events, assuming the standard model. One may hope to eventually reduce the errors on  $m_t$  to half a percent or better, while determining  $\alpha_s$  unambiguously to a few percent. With a larger number of events, it will be possible to measure  $\Gamma_t$  to perhaps 20%. Determinations of the quantities  $m_H$  and  $g_{tH}$ , though imprecise, will still be of great importance as tests for nonminimal Higgs sectors. In summary, it is evident that the ability to correctly predict the entire  $t\bar{t}$  threshold cross section at the level of a few percent will be an important and detailed test of the standard model, or of any other model which is offered to replace it.

### ACKNOWLEDGMENTS

We thank members of the theory group and of the Next Linear Collider group at the Stanford Linear Accelerator Center for many helpful discussions. We are especially grateful to S. Brodsky and B. Warr for helping us understand various theoretical subtleties, and to T. Barklow, D. Burke, and S. Komamiya for giving us insight into the relevant experimental considerations. We are also grateful to W. Kwong and J. Rosner for bringing their work to our attention. This work was supported by the Department of Energy, contract DE-AC03-76SF00515. M.J.S. was supported in part by the NSF Graduate program.

<sup>1</sup>CDF Collaboration, F. Abe *et al.*, Phys. Rev. Lett. **64**, 142 (1990).

<sup>2</sup>I. I. Y. Bigi, Yu. L. Dokshitzer, V. Khoze, J. Kühn, and P. Zerwas, Phys. Lett. B **181**, 157 (1986).

<sup>3</sup>V. S. Fadin and V. A. Khoze, Pis'ma Zh. Eksp. Teor. Fiz. **46**, 417 (1987) [JETP Lett. **46**, 525 (1987)]; Yad. Fiz. **48**, 487 (1988) [Sov. J. Nucl. Phys. **48**, 309 (1988)].

<sup>4</sup>E. Eichten, K. Gottfried, T. Kinoshita, J. Kogut, K. D. Lane, and T.-M. Yan, Phys. Rev. Lett. **34**, 369 (1975); **36**, 1276(E) (1976).

<sup>5</sup>H. Inazawa and T. Morii, Phys. Lett. B **203**, 279 (1988); **207**, 520(E) (1988); H. Inazawa, T. Morii, and S. Tanaka, Z. Phys. C **43**, 569 (1989).

<sup>6</sup>W. Kwong, this issue Phys. Rev. D **43**, 1488 (1991).

<sup>7</sup>J. Feigenbaum, Phys. Rev. D **43**, 264 (1991).

<sup>8</sup>One unit of  $R = 4\pi\alpha_{\text{QED}}^2/3s$ , the point cross section for  $e^+e^- \rightarrow \mu^+\mu^-$ . For an integrated luminosity of  $10^{40}$  cm<sup>-2</sup> at a center-of-mass energy of 300 GeV, 1 R = 9600 events.

<sup>9</sup>R. Barbieri, R. Gatto, R. Kögerler, and Z. Kunzst, Phys. Lett. **57B**, 455 (1975).

- <sup>10</sup>W. Buchmüller and S. H. H. Tye, *Phys. Rev. D* **24**, 132 (1981).
- <sup>11</sup>W. Fischler, *Nucl. Phys.* **B129**, 157 (1977).
- <sup>12</sup>A. Billoire, *Phys. Lett.* **92B**, 343 (1980).
- <sup>13</sup>W. Buchmüller, G. Grunberg, and S. H. H. Tye, *Phys. Rev. Lett.* **45**, 103 (1980); **45**, 587(E) (1980).
- <sup>14</sup>C. Quigg and J. L. Rosner, *Phys. Rep. C* **56**, 167 (1979).
- <sup>15</sup>To evaluate electroweak effects, we have used the parameters  $m_Z=91.17$  GeV,  $m_W=80.00$  GeV,  $m_b=5.0$  GeV, and  $\sin^2\theta_W=0.235$ . Of these parameters, only  $m_W$  has a significant effect on the  $t\bar{t}$  cross section, through its influence on the top-quark width.
- <sup>16</sup>H. Burkhardt, F. Jegerlehner, G. Penso, and C. Verzegnassi, *Z. Phys. C* **43**, 497 (1989).
- <sup>17</sup>E. A. Kuraev and V. S. Fadin, *Yad Fiz.* **41**, 733 (1985) [*Sov. J. Nucl. Phys.* **41**, 466 (1985)].
- <sup>18</sup>F. Berends, in *Z Physics at LEP 1*, proceedings of the Workshop, Geneva, Switzerland, 1989, edited by G. Altarelli, R. Kleiss, and C. Verzegnassi, (CERN Yellow Report No. 89-08, Geneva, 1989), Vol. 1.
- <sup>19</sup>M. E. Peskin, in *Physics at the 100 GeV Mass Scale*, proceedings of the Seventeenth SLAC Summer Institute on Particle Physics, Stanford, California, 1989, edited by E. C. Brennan, (SLAC Report No. 361, Stanford, 1990).
- <sup>20</sup>S. Komamiya, SLAC Report No. SLAC-PUB-5324, 1990 (unpublished).
- <sup>21</sup>S. Komamiya (private communication).